

---

This is an electronic reprint of the original article.  
This reprint may differ from the original in pagination and typographic detail.

Hakula, Harri

## Harmonic extension elements : Eigenproblems and error estimation

*Published in:*  
Computers and Mathematics with Applications

*DOI:*  
[10.1016/j.camwa.2024.03.012](https://doi.org/10.1016/j.camwa.2024.03.012)

Published: 01/06/2024

*Document Version*  
Publisher's PDF, also known as Version of record

*Published under the following license:*  
CC BY

*Please cite the original version:*  
Hakula, H. (2024). Harmonic extension elements : Eigenproblems and error estimation. *Computers and Mathematics with Applications*, 163, 27-41. <https://doi.org/10.1016/j.camwa.2024.03.012>

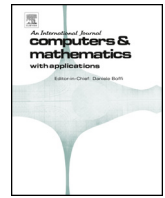
---

This material is protected by copyright and other intellectual property rights, and duplication or sale of all or part of any of the repository collections is not permitted, except that material may be duplicated by you for your research use or educational purposes in electronic or print form. You must obtain permission for any other use. Electronic or print copies may not be offered, whether for sale or otherwise to anyone who is not an authorised user.



Contents lists available at ScienceDirect

## Computers and Mathematics with Applications

journal homepage: [www.elsevier.com/locate/camwa](http://www.elsevier.com/locate/camwa)

## Harmonic extension elements: Eigenproblems and error estimation

Harri Hakula

Aalto University, Department of Mathematics and Systems Analysis, Otakaari 1, 00076, Aalto, Finland

## ARTICLE INFO

## Keywords:

Harmonic functions  
Finite elements  
hp-FEM  
Eigenproblems

## ABSTRACT

A non-intrusive extension to the standard  $p$ -version of the finite element method, so-called harmonic extension elements, is studied in the context of eigenproblems. The standard polynomial shape functions are replaced where appropriate with harmonic extensions of the boundary restrictions of the standard shape functions or solutions to a local Poisson problem. The reference elements are adapted to include extensions in order to ensure a conforming discretisation even if the meshes are not conforming. The hierarchic structure of the extension basis means that auxiliary space error estimators of the  $p$ -version of the finite element method are directly applicable. The additional computational workload in construction of the required extensions can be reduced using symmetries and multimesh techniques. The numerical experiments demonstrate the efficiency of the proposed extension resulting in exponential convergence in the quantities of interest if the mesh is properly graded.

## 1. Introduction

In modern engineering simulations geometry handling remains a challenge. In short, complicated domains often lead to expensive simulations. Similarly the solution itself may have characteristic features such as singularities and boundary layers that have to be taken into account a priori. In recent years many new ways of addressing the discretisation of the underlying partial differential equations (PDEs) have been introduced. The methods can either be continuous or discontinuous, even if the problem itself is continuous, or alternatively, the domain discretisations can either be simplicial or polygonal and not necessarily conforming. Notable examples of new developments are virtual elements [1] and the so-called hybrid high-order method [2]. CutFEM is an approach where the initial discretisations are not conforming, that is, they are unfitted [3]. The method is on solid theoretical foundation, see a recent study [4] which contains a brief overview relating it to other approaches such as the finite cell method [5] and isogeometric methods with trimmed elements [6]. Also, in the Multi-scale FEM the base functions are adapted to the local properties of the differential operator, which is advantageous in problems with rapidly oscillating coefficients [7], [8].

In this paper the focus is on eigenproblems and their resolution with so-called adaptive reference elements, an  $hp$ -finite element method (FEM) (see e.g. [9], [10]) where a conforming formulation is constructed on a non-conforming mesh by adapting the shape functions

as harmonic extensions. It has been previously applied to model problems with Dirichlet-Neumann boundary singularities [11], and elasticity problems with strong boundary layers [12]. The theoretical foundations for the method can be directly adopted from Weißer's work on boundary element based FEM [13], [14]. Ovall and collaborators have further extended these ideas with impressive results [15], [16]. The DPG method of Demkowicz and Gopalakrishnan [17] also includes the fundamental concept of computable shape functions. Here the term computable function is defined as something for which an algorithm exists even though an explicit expression cannot be defined.

The fundamental design principle of adaptive reference elements is to preserve the existing  $p$ - and  $hp$ -finite element software infrastructure. New shape functions are introduced as computable entities which are compatible with the standard high order shape functions yet enable very general mesh grading within the reference element framework. In short, finite elements are implemented with finite elements. However, the extensions are defined only on reference elements. This means that the mapping of the reference elements has to fall back to standard methods such as blending functions. A highly advantageous consequence of this is that curved elements are included without any extra effort.

Every element can have arbitrary number of nodes, but not every subdivision of edges or faces is admissible. Only those elements that can be represented as mapped reference elements are valid. This in turn

E-mail address: [Harri.Hakula@aalto.fi](mailto:Harri.Hakula@aalto.fi).

<https://doi.org/10.1016/j.camwa.2024.03.012>

Received 14 July 2023; Received in revised form 1 February 2024; Accepted 9 March 2024

Available online 26 March 2024

0898-1221/© 2024 The Author. Published by Elsevier Ltd. This is an open access article under the CC BY license (<http://creativecommons.org/licenses/by/4.0/>).

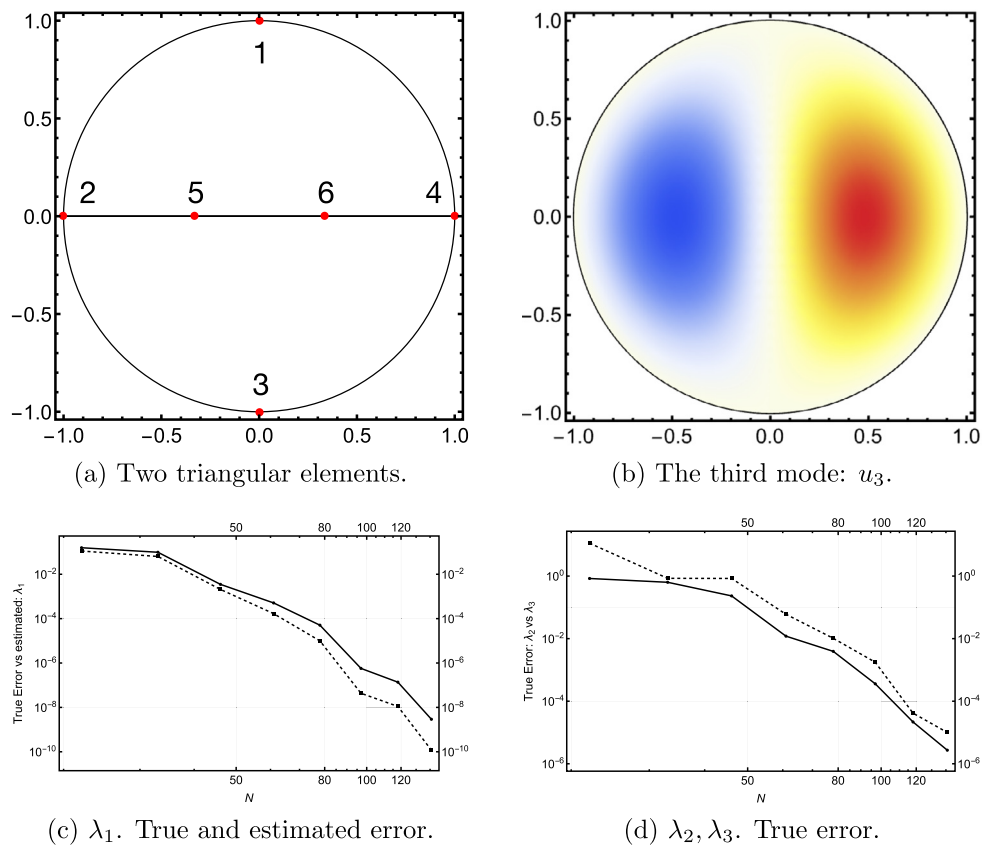


Fig. 1. Eigenmodes on a unit disk. (a) Two triangular elements with mapping nodes  $\{1, 2, 4\}$  and  $\{2, 3, 4\}$ , respectively. True and estimated errors over a  $p$ -sequence. (c) Convergence graphs: Solid line: true error, Dashed: estimated error. (d) Convergence graphs: Solid line: true error of  $\lambda_2$ , Dashed: true error of  $\lambda_3$ .

requires that on each element a set of nodes is designated as those defining the mapping, in other words, whether for example in 2D an element is a triangle or quadrilateral. The choice of the mapping is not unique. The standard implementation within the  $p$ -community as mentioned above is the blending function method [18], but any of the modern numerical conformal mapping methods would be equally suited to the task [19]. In the standard formulation the nodes that do not define the mapping are called hanging nodes. Within the framework presented here there are no hanging nodes, but the space of basis functions is enriched so that every configuration results in a conforming formulation.

Since the proposed method is an extension of the  $p$ -FEM, one should expect similar performance. In Fig. 1 some convergence results on a simple reference problem, a circular membrane, are shown. The second and third eigenmodes are known to have the same eigenvalues, and hence the corresponding eigenmodes will span the subspace. In order to resolve this particular subspace accurately one should have a mesh that preserves rotational symmetry. The mesh in Fig. 1a is designed on purpose not to possess this property so that the two modes cannot in the given case be resolved with the same accuracy. With this simple setup the first eigenvalue converges exponentially (Fig. 1c), whereas within the cluster  $\lambda_{2,3}$  there is slight deterioration in the constant. In this instance it happens that the second mode is perfectly aligned with the meshlines, but the third one is not (Fig. 1b), which explains the difference.

In the numerical experiments below, examples with singularities will be considered. There the flexibility of the extension is fully utilised. The main contribution of this work is to demonstrate that the proposed method has the same convergence characteristics as the standard  $hp$ -FEM and in a similar geometric setting is more efficient in terms of degrees of freedom. Furthermore, the auxiliary space error estimators are naturally applicable also in the eigenproblem setting. One of the

properties of the method that sets it apart from the standard method is that it is possible to have a boundary singularity on an element edge. Numerical evidence indicates that in such a case the convergence is algebraic as in the comparable  $p$ -FEM. Finally, possibilities of reducing the computational effort in construction of the shape functions are discussed.

The rest of the paper is structured as follows: In Section 2 the concept of adaptive reference elements is introduced, how the shape functions differ from the standard  $p$ -FEM shapes is described, and the direct adaptation of the auxiliary subspace error estimation is outlined. The actual implementation details of the adaptive reference elements are discussed in detail in Section 3. This includes the use of symmetries in reducing the computational work. The open question of design of efficient quadrature rules is briefly outlined. The numerical experiments in Section 4 cover cases with singularities. In the Pacman problem the mesh has been adapted a priori to achieve exponential convergence, but in the Padovan spiral, where the singularity is located on the boundary of an adaptive element, this has not been done in order to demonstrate the predicted algebraic rate of convergence. The effect of the shape resolution, that is, the numerical accuracy of the shape function is also studied in the context of the numerical experiments. Finally, the conclusions are summarised in Section 5.

## 2. Preliminaries

In this section the background concepts, such as the construction of the 2D adaptive reference elements, are introduced. Familiarity with the basic concepts of the  $p$ - and  $hp$ -versions of the finite element method is assumed. The  $hp$ -solver is implemented with Mathematica [20] – for its design principles, see [21].

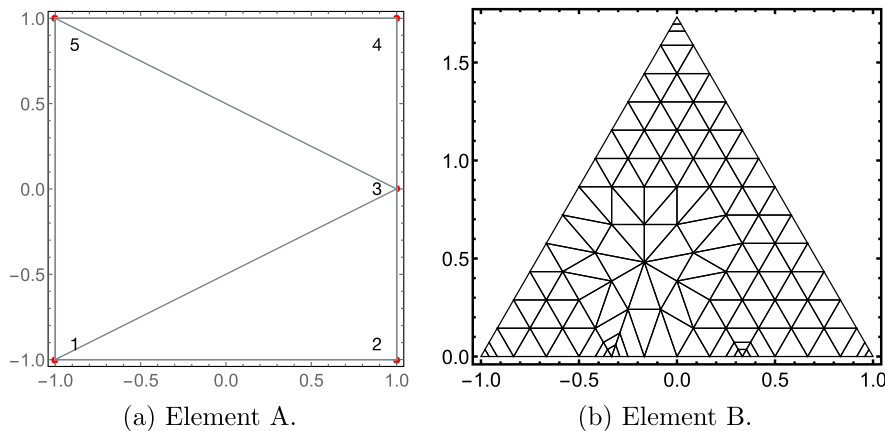


Fig. 2. Adaptive reference elements (A and B). (a) Quadrilateral with five nodes. Minimal implementation mesh with three triangles. The element mapping is defined using the four corner nodes only. (b) Triangle with five nodes. Refined implementation mesh.

2.1. Adaptive reference elements

As usual in finite elements every element is an instance of some reference element. To fix terminology every adaptive element (AE) is said to be an instance of an adaptive reference element (ARE). The adaptive reference element is defined with a set of points or nodes as usual. What is different is that only a subset of nodes is used to define the mapping of the element.

Let us consider the examples in Fig. 2, where two adaptive reference elements, one quadrilateral and one triangle, are shown. The elements have five nodes, divided into mapping nodes and edge nodes. This choice is not unique, however. For instance, the adaptive reference element (ARE) corresponding to Element A could be a triangle with mapping nodes {1,2,4} and two edge (hanging) nodes 3 and 5, where the edge {1,5,4} would be curved and passing through 5. The implementation mesh of Element B includes refinements to corners and nodal points of the bottom edge. Naturally, computations on Element B are much more expensive, yet with higher accuracy. As always in numerical analysis, balancing of error sources is necessary for optimal performance, and within the proposed extension there is an inbuilt possibility of relaxing the accuracy of the shapes and associated inner products within the solution process.

This discussion can be condensed into the following definition:

**Definition 1 ([11]).** (Planar adaptive reference element (ARE)) Given a set of points  $K$ ,  $|K| \geq 3$ , any partition of  $K$  into mapping and edge nodes is admissible, if the edge nodes lie on the boundary of some valid (univalent) mapping of the standard reference element defined by the mapping points. This partition defines the adaptive reference element. If the set of edge nodes is empty, the adaptive reference element is equivalent to a standard element.

2.2. Shape functions

The shape functions are computed as harmonic extensions of the restrictions of the standard FEM nodal and edge functions on the element boundary. Here we follow closely the discussion in [11]. In other words, for any standard nodal or edge shape function  $\phi(x, y)$  we compute its harmonic extension  $\varphi(x, y)$ :

$$\begin{cases} \Delta \varphi(x, y) = 0, & \text{in } K, \\ \varphi(x, y) = \phi(x, y)|_{\partial K}, & \text{on } \partial K, \end{cases} \quad (1)$$

where  $K$  is either a reference quadrilateral or triangle. Some examples of such shape functions including derivatives are given in Figs. 3 and 4. This construction guarantees a continuous formulation combining

AEs and standard finite elements. Also notice, that the nodal modes automatically form a partition of unity.

For instance, in the case of Fig. 2 the nodal shape function associated with the node 3 is computed by setting the restriction  $\phi(1, y)|_{\partial K}$  over the edge at  $x = 1$  to be the standard linear hat function with  $\phi(1, 0)|_{\partial K} = 1$ .

The associated inner modes  $\hat{\varphi}(x, y)$  are the functions satisfying

$$\begin{cases} \Delta \hat{\varphi}(x, y) = q(x, y), & \text{in } K, \\ \hat{\varphi}(x, y) = 0, & \text{on } \partial K, \end{cases} \quad (2)$$

where  $q(x, y)$  is some polynomial. For instance  $q(x, y) = 1$  (constant) induces a standard bubble function. The set of elemental inner modes  $\hat{\varphi}(x, y)_K$  is constructed with products of Legendre polynomials, that is, all  $q(x, y) \in q(x, y)_K$ , where  $q(x, y)_K = \{P_i(x)P_j(y), i = 0, \dots, p - 2, j = 0, \dots, p - 2\}$ . With this choice the number of inner modes is the same as with the standard  $p$ -FEM, although the approximation properties are not. There exists a family of polynomials that could be used instead of the computed ones (see [16]).

The computation of the shape functions is done with finite elements (naturally!). Hence, the concept of the implementation mesh arises, or more precisely, implementation discretisation. In order to simplify the evaluation of the inner products between the shape functions, every shape function associated with a given element is computed using the same implementation discretisation. One consequence of this is that the same extension may be computed using many different implementation discretisations. This is discussed in more detail below.

2.3. Error estimation

Since the harmonic extension method is a non-intrusive extension of the  $p$ -FEM, it is natural to apply the existing a posteriori error estimation techniques directly. In particular, the auxiliary subspace methods are natural candidates [22], [23]. The discussion here is adapted from [23].

Formally, we are concerned with the a posteriori estimation of error in high-order ( $p$  or  $hp$ ) finite element approximations of eigenvalues and invariant subspaces for variational eigenvalue problems of the form: Find  $(\lambda, \psi) \in \mathbb{R} \times \mathcal{H}$ ,  $\psi \neq 0$ , satisfying

$$\underbrace{\int_{\Omega} \nabla \psi \cdot \nabla v \, dx}_{B(\psi, v)} = \lambda \underbrace{\int_{\Omega} \psi v \, dx}_{(\psi, v)} \text{ for all } v \in \mathcal{H}, \quad (3)$$

where  $\Omega \subset \mathbb{R}^d$  is open and bounded, and  $\mathcal{H} \subset H^1(\Omega)$  incorporates homogeneous Dirichlet, Neumann, or mixed Dirichlet/Neumann boundary

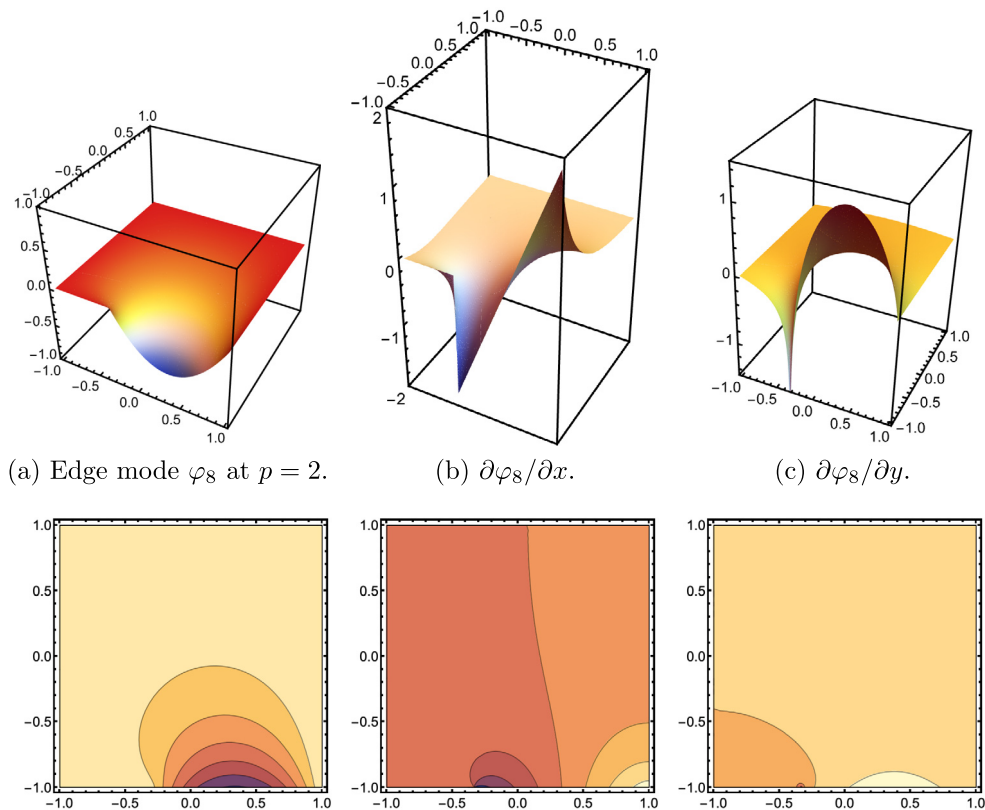


Fig. 3. Quadrilateral. Quadratic edge mode and its partial derivatives on the reference domain.

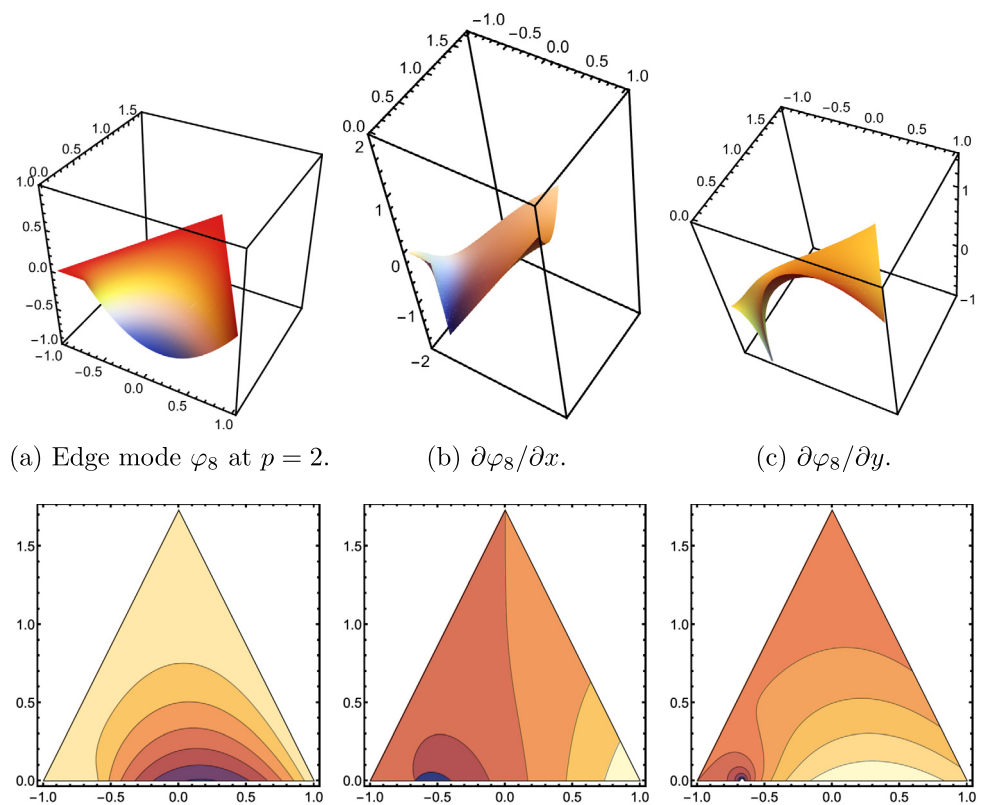


Fig. 4. Triangle. Quadratic edge mode and its partial derivatives on the reference domain.

conditions.  $B$  is an inner-product on  $\mathcal{H}$ , whose induced “energy” norm,  $\|v\| = \sqrt{B(v, v)}$ , is equivalent to the standard norm on  $H^1(\Omega)$ ,  $\|v\|_1$ . We also use  $\|v\|_0$  to denote the standard norm on  $L^2(\Omega)$ .

The basic idea is to construct error estimates for eigenvalue problems by building upon those for source problems. More specifically we see that an a posteriori estimate of  $\|u(f_j) - \hat{u}(f_j)\|$ , where the “source”  $f_j = \hat{\mu}_j \hat{\phi}_j$  is obtained from the approximate eigenpair  $(\hat{\mu}_j, \hat{\phi}_j)$ , provides a measure of how far  $\hat{\phi}_j$  is from a true eigenvector and how far  $\hat{\mu}_j$  is from a true eigenvalue. The field of a posteriori error estimation for source problems, particularly for the reaction-diffusion operators we consider here, is quite mature, so we have many well-documented methods for estimating  $\|u(f_j) - \hat{u}(f_j)\|$ .

Given  $f \in L^2(\Omega)$ , the exact and finite element solutions,  $u(f) \in \mathcal{H}$  and  $\hat{u}(f) \in V$ , satisfy

$$B(u(f), v) = (f, v) \text{ for all } v \in \mathcal{H} \quad , \quad B(\hat{u}(f), v) = (f, v) \text{ for all } v \in V \quad .$$

We compute an approximate error function  $\varepsilon(f) \in W$  in an auxiliary subspace  $W \subset \mathcal{H}$  as the projection of  $u(f) - \hat{u}(f)$  onto  $W$ ,

$$B(\varepsilon(f), v) = B(u(f) - \hat{u}(f), v) = (f, v) - B(\hat{u}(f), v) \text{ for all } v \in W \quad . \quad (4)$$

The error space  $W$  is chosen so that  $V \cap W = \{0\}$ ,  $W$  is defined on the same mesh as  $V$ , and  $V \oplus W$  is a richer approximation space on this mesh. We adopt the approach suggested in [22] for problems in 2D, which we describe at the level of elements. If element functions of degree  $m$  are used on an element  $T$  in  $V$ , then element functions of degree  $m + 2$  are used on this same element in  $W$ . If edge functions of degree  $m$  are used on an edge  $e$  in  $V$ , then edge functions of degree  $m + 1$  are used on this same edge in  $W$ . We slightly rephrase [22, Theorem 1.4] in our context for the energy norm. We take  $\mathcal{E}$  to be the set of edges of the mesh that are not on the Dirichlet part of the boundary, and define the volumetric residual,  $R_T = f - (-\nabla \cdot \nabla \hat{u}(f))|_T$ . When  $e \in \mathcal{E}$  is an interior edge, we define the edge residual as  $r_e = (\nabla \hat{u}(f) \cdot \mathbf{n}_T)|_T + (\nabla \hat{u}(f) \cdot \mathbf{n}_{T'})|_{T'}$ , where  $T$  and  $T'$  are the cells sharing this edge, and  $\mathbf{n}_T$  and  $\mathbf{n}_{T'}$  are their outward unit normals. For a Neumann boundary edge, we define the edge residual as  $r_e = (\nabla \hat{u}(f) \cdot \mathbf{n}_T)|_T$ . With these definitions in hand, we can state the theorem.

**Theorem 1.** *There is a constant  $c$ , depending on the shape-regularity of  $\mathcal{T}$  and the polynomial degree  $p$  such that*

$$\|\varepsilon(f)\| \leq \|u(f) - \hat{u}(f)\| \leq c (\|\varepsilon(f)\| + \text{osc}(R, r, \mathcal{T})) \quad ,$$

where the residual oscillation is defined by

$$\begin{aligned} \text{osc}(R, r, \mathcal{T})^2 &= \sum_{T \in \mathcal{T}} h_T^2 \inf_{\kappa \in \mathbb{Q}_{p-1}(T)} \|R_T - \kappa\|_{L^2(T)}^2 \\ &+ \sum_{e \in \mathcal{E}} |e| \inf_{\kappa \in \mathbb{Q}_{p-1}(e)} \|r_e - \kappa\|_{L^2(e)}^2 \quad , \end{aligned}$$

where  $h_T$  and  $|e|$  are the diameter of  $T$  and length of the edge  $e$ , respectively.

The proof given in [22] was given for simplicial meshes, but its performance was rigorously tested for more general meshes. It must be pointed out that even though there is compelling numerical evidence that  $c$  is independent of  $p$ , such independence has not been theoretically established.

### 3. Implementation of adaptive reference elements

In many cases the mesh refinements are structured. In particular in higher-order FEM context geometric refinement to a corner or edge is a prime example. In our setting this kind of mesh refinement is easy to implement since it can be done using simple replacement rules.

Having multiple elements with exactly the same subdivisions makes it natural to search for ways of classifying elements in order to minimise

the work load. One such method is assigning a type for each element. For constant coefficient problems one reference element is computed per every type, which makes the final assembly efficient.

In this work the emphasis is on arbitrary subdivisions of element edges. An unfortunate consequence of this is that there can easily be a combinatorial expansion of types and the benefits of the scheme are not realisable. The solution is to borrow the idea advocated by Demkowicz [24], where the focus is shifted from the element level to that of the individual shapes.

Every edge shape has its support on the edge, and is defined by its parity and the associated polynomial order. Naturally, each shape can be included in elements of multiple types. In standard  $p$ -FEM this poses no problems since the shape functions are defined analytically. Here, the shape is represented as a FEM solution or harmonic function on some discretisation of the domain of the reference element. If the number of element types is small, the shapes can be recomputed for each reference element with the added benefit that each shape of the element can be realised on the same mesh. In the general case, the shapes are projected onto the elemental discretisation. There are different ways of accomplishing this, for instance the multimesh approach [25].

#### 3.1. Type of reference element

In order to minimise computational work, it is necessary to introduce a way to maintain bookkeeping for the evaluated shape functions and AREs. The idea of a type of an element was introduced in [21], where it was motivated by the need of speeding up computations in a high-level programming environment. Since compatibility with the standard  $p$ -FEM is required (or desired), on split edges the shape functions must have correct parities.

Legendre polynomials of degree  $n$  can be defined using a recursion formula

$$(n + 1)P_{n+1}(x) - (2n + 1)xP_n(x) + nP_{n-1}(x) = 0, \quad P_0(x) = 1. \quad (5)$$

For our purposes the central polynomials are the integrated Legendre polynomials for  $\xi \in [-1, 1]$

$$\phi_n(\xi) = \sqrt{\frac{2n-1}{2}} \int_{-1}^{\xi} P_{n-1}(t) dt, \quad n = 2, 3, \dots \quad (6)$$

which can be rewritten as linear combinations of Legendre polynomials

$$\phi_n(\xi) = \frac{1}{\sqrt{2(2n-1)}} (P_n(\xi) - P_{n-2}(\xi)), \quad n = 2, 3, \dots \quad (7)$$

The normalizing coefficients are chosen so that

$$\int_{-1}^1 \frac{d\phi_i(\xi)}{d\xi} \frac{d\phi_j(\xi)}{d\xi} d\xi = \delta_{ij}, \quad i, j \geq 2. \quad (8)$$

Therefore, the  $\phi_n(\xi)$  inherit the property of the Legendre polynomials,

$$\phi_n(\xi) = (-1)^n \phi_n(-\xi). \quad (9)$$

This means that every edge has to be oriented in such a way that the shape function has a consistent sign or parity on both elements sharing it.

In the following it is assumed that every partition of edges is regular. For every element a type is assigned in the following way: First a mapping node with the smallest identifier is chosen and the simplex is rotated so that the selected node is in a fixed position (normalisation); next for each edge, the parameter range of its support on the reference element is derived; finally each edge segment is assigned a parity by comparing the identifiers of the end points. Thus every edge, split or not, has its contribution to the type of the ARE in form of a tuple  $(s, [a, b])$ , where  $s = \pm 1$ , and  $-1 \leq a < b \leq 1$ . For instance, the ARE of

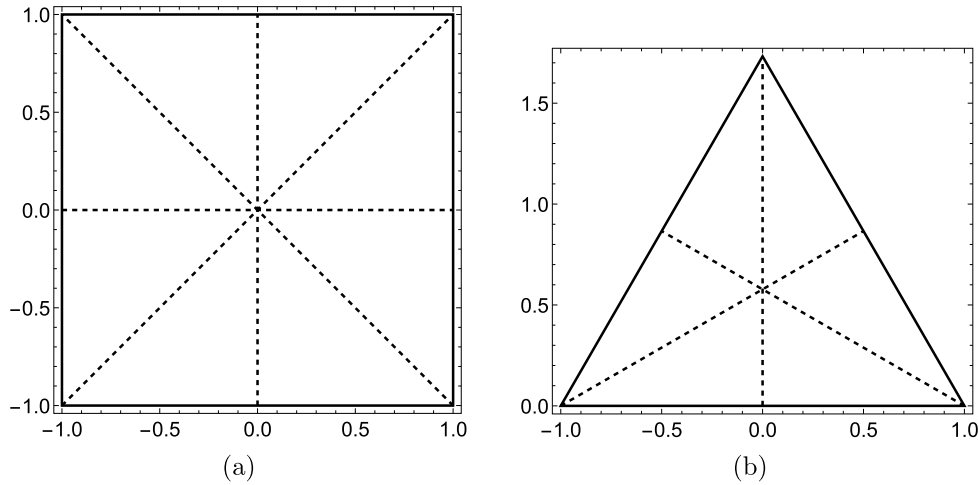


Fig. 5. Two reference domains with symmetry axes indicated with dashed lines.

Fig. 2 has the type  $S_Q$  – assuming that the nodes are identified as in the picture –

$$S_Q = ((1, [-1, 1]), ((1, [-1, 0]), (1, [0, 1]), (1, [-1, 1]), (-1, [-1, 1])). \quad (10)$$

The convention is that the positive direction is from the node with the smallest identifier. For standard  $p$ -FEM quadrilaterals there are four types, and for triangles two types, in both cases assuming that the inner modes need not have an orientation. The inner modes are always assumed to be oriented in the same way, that is, they do not affect the type. If the edge partitions are not regular, then the type has to be augmented with some coordinate information.

### 3.2. Symmetry groups

If an edge shape is defined as its own entity on one edge, it follows that it can be mapped to every other edge as well using symmetry transformations.<sup>1</sup> This could be done in the standard  $p$ -FEM setting as well – it is just so much more convenient to use the analytic expressions.

Let us consider a reference triangle and edge shapes of  $p = 3$ . The edges are labelled as follows (not unique): Edge 1:  $(-1, 0) \rightarrow (1, 0)$ , Edge 2:  $(1, 0) \rightarrow (0, \sqrt{3})$ , Edge 3:  $(-1, 0) \rightarrow (0, \sqrt{3})$ . On Edge 1 the corresponding shape has the expression

$$\varphi_3^1(\xi, \eta) = \frac{1}{6} \sqrt{\frac{5}{2}} \xi (3\xi^2 - \eta^2 + 2\sqrt{3}\eta - 3).$$

On Edge 2 we have

$$\varphi_3^2(\xi, \eta) = \frac{1}{6} \sqrt{\frac{5}{6}} \eta (-3\xi + \sqrt{3}\eta - 3) (-\xi + \sqrt{3}\eta - 1).$$

The centroid of the reference triangle is  $x_0 = (0, 1/\sqrt{3})$ . Edge 1 can be rotated onto Edge 2 by rotation about the centroid by  $\theta = 2\pi/3$ . This affine map is

$$F : x \rightarrow x', \quad x, x' \in \mathbb{R}^2, \quad x' = F(x) = A(x - x_0) + x_0,$$

$$A = \frac{1}{2} \begin{pmatrix} -1 & -\sqrt{3} \\ \sqrt{3} & -1 \end{pmatrix},$$

where the rotation matrix is denoted by  $A$ . Therefore  $\varphi_3^2(\xi, \eta) = \varphi_3^1(\xi', \eta')$ , where  $(\xi', \eta') = F(-\xi, \eta)$  to preserve the right parametrisation.

<sup>1</sup> One does not normally apply abstract algebra in a finite element context.

Derivatives can be mapped similarly using the chain rule. Formally

$$\nabla \varphi_3^2(\xi, \eta) = A^T \nabla \varphi_3^1(\xi', \eta').$$

The symmetry transformation groups  $\triangle_G$  and  $\square_G$ , for triangles and quadrilaterals, respectively, consist of rotations and reflections. The symmetry axes are indicated in Fig. 5.

### 3.3. Implementation discretisations

In Fig. 2 the meshes used in construction of the two adaptive reference elements are shown. One of them is minimal and the other one a priori adapted. In Fig. 6 a simple example of an implementation discretisation conforming to the symmetry group is illustrated.

The edge shapes computed on Fig. 6a are rotated and reflected onto the mesh in Fig. 6b. The large elements with possible large angles can be assigned higher polynomial orders if necessary. Of course, there are practical limits to how small edge sections at the nodes can be implemented while preserving symmetries in the discretisation. There is always the fallback option of using separate discretisations per element.

In the standard  $p$ -FEM the shape functions are given exactly. Here a new type of discretisation error is introduced, namely shape discretisation or implementation error. More careful analysis of the effects of this error is required. In the numerical experiments below this question is discussed in relation to different features of the solutions.

### 3.4. Quadrature design

In Figs. 3 and 4 the contour plots give an idea of how the “masses” of the shapes and derivatives are distributed. It is intuitively clear that standard quadrature rules are ineffective since the inner products are localised in terms of  $L^2$ -norms, say. The practical choice in the absence of any adapted quadrature rules is to use the implementation discretisations and construct a composite rule. This of course becomes more expensive as the implementation discretisation is refined. Notice that even if the PDE is a constant coefficient one, curved boundaries will force one to apply quadrature rules.

## 4. Numerical experiments

The model problem is the Laplace eigenvalue problem:

$$-\Delta \psi = \lambda \psi \text{ in } \Omega, \quad \psi = 0 \text{ on } \Gamma, \quad \Gamma \subseteq \partial \Omega.$$

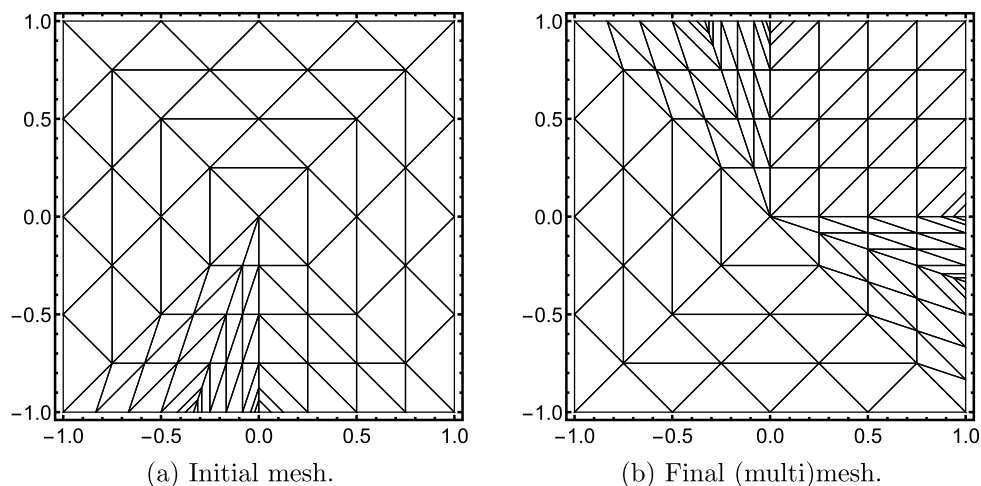


Fig. 6. Symmetries in action. (a) Initial mesh used to evaluate the edge shapes. (b) Final mesh used in the application where the edge shapes are both rotated to the right edge and reflected to the top edge.

Table 1

Discretisation data. Uniform  $p = 12$ . Nodes, Edges, Triangles ( $p$ -FEM), ARE Triangles, ARE Quadrilaterals, and the number of degrees of freedom.

Example	N	E	T	ARE T	ARE Q	#DOF
Pacman/Slit Disk	118	169	-	4	48	8005
Padovan Spiral	15	27	4	9	-	1027

The first and reference problem is the so-called Pacman-problem, where the exact eigeninformation is known. The second problem is actually a sequence of problems resulting from a geometric representation of an integer sequence known as the Padovan sequence. The topological entities in the meshes are tabulated in Table 1 (the Padovan Spiral data refers to the final configuration). In all cases the computed reference results are done with an  $hp$ -implementation as in [23]. Included in the experiments is the investigation of the accuracy with which the harmonic extension shape functions have been evaluated. We distinguish between the true error, when the exact reference value is known, the error, when the reference value is a computed one, and the estimated error based on the auxiliary space error estimator introduced in Section 2.3. Our measure of “quality” of the estimate is the so-called effectivity index which the ratio of the estimated error and the error, either true or computed. Also, since the shape functions are themselves computed quantities, we consider the concept of error improvement where the effect of higher resolution (accuracy) of the shapes on the quantity of interest, such as an eigenvalue, is measured.

4.1. Pacman and Slit Disk

Fix  $\alpha \in (1/2, 1)$  and let  $\Omega \subset \mathbb{R}^2$  be the sector of the unit disk for which  $0 < r < 1$  and  $0 < \theta < \pi/\alpha$ , where  $r$  and  $\theta$  are the usual polar coordinates. For illustrations, see Fig. 7. The eigenvalues and vectors are known explicitly (cf. [26]), and are doubly-indexed for  $m, n \in \mathbb{N}$  by

$$\psi_{m,n} = J_{\sigma_m}(j_n(\sigma_m)r) \sin(\sigma_m\theta), \quad \lambda_{m,n} = [j_n(\sigma_m)]^2, \quad \sigma_m = m\alpha, \quad (11)$$

where  $J_{\sigma_m}$  is the first-kind Bessel function of order  $\sigma_m$  and  $j_n(\sigma_m)$  is the  $n$ th positive root of  $J_{\sigma_m}$ .

For the special case of  $m = 1$  and  $\alpha = 1/2$ , i.e., the Slit disk, we get  $J_{1/2}(z) = \sqrt{2/(\pi z)} \sin z$ , and observe that  $\lambda_{m,1} = (m\pi)^2$ , and  $\psi_{m,1} \in H^{3/2-\epsilon}(\Omega)$  only for  $\epsilon > 0$ .

The domains and the geometrically refined meshes are shown in Fig. 7. Everything is based on a priori information of the type of singularity and modes. The choice of concentrating on eigenpairs  $(\lambda_1, u_1)$  and  $(\lambda_6, u_6)$  is not arbitrary, they are the first two modes affected by the singularity at the origin. This is illustrated in Figs. 8 and 9.

One would expect the convergence rate to be of the same rate as with the  $hp$ -FEM. This proves to be the case, and due to more efficient discretisation of the domain, the constant is better for the harmonic extensions. The auxiliary space estimator also performs as expected and as is optimistic as is typical for this class of estimators. These results are aligned with those of [23].

In Figs. 10 and 11 for both eigenvalues the comparison with the  $hp$  and the effectivity indices are shown. The  $p$ -sequence run from  $p = 2, \dots, 10$ , and maximal evaluated degree of polynomials is  $p_{\max} = 12$  to accommodate the auxiliary error estimator. Interestingly, the asymptotic convergence rate is reached at  $p = 5$ . For  $\lambda_1$  the effectivity index is practically constant after  $p = 5$ , but there is some oscillation for  $\lambda_6$  as is expected since it is more difficult to approximate.

4.2. Padovan spiral

The Padovan sequence is the sequence of integers  $P(n)$ ,  $n \in \mathbb{N}$ , defined by the initial values

$$P(0) = P(1) = P(2) = 1,$$

and the recurrence relation

$$P(n) = P(n - 2) + P(n - 3).$$

Padovan sequence was named by I. Stewart [27] after R. Padovan, who first described it in his book [28]. Consider Fig. 12, where the Padovan sequence is used to generate a spiral of equilateral triangles with edges length following the  $P(n)$  sequence (unit length = 2, as defined by the reference triangle). We are interested in the eigenvalues of the spiral or horn, whose boundary is indicated with thick lines. For completeness’ sake we also consider the full Dirichlet case, where the whole outer boundary is fixed. In fact, the Padovan sequence induces a sequence spirals as seen from the figure.

This example is of special interest since the split edges have (almost) unique subdivisions, that is, each element has a unique type. We observe for the divided edges

$$1 : 1, 1 : 2, 1 : 3, 1 : 5, 2 : 5, 2 : 7, 3 : 9, 4 : 12, 5 : 16,$$

where only  $1 : 3 = 3 : 9 = 4 : 12$  is repeated over the sequence.

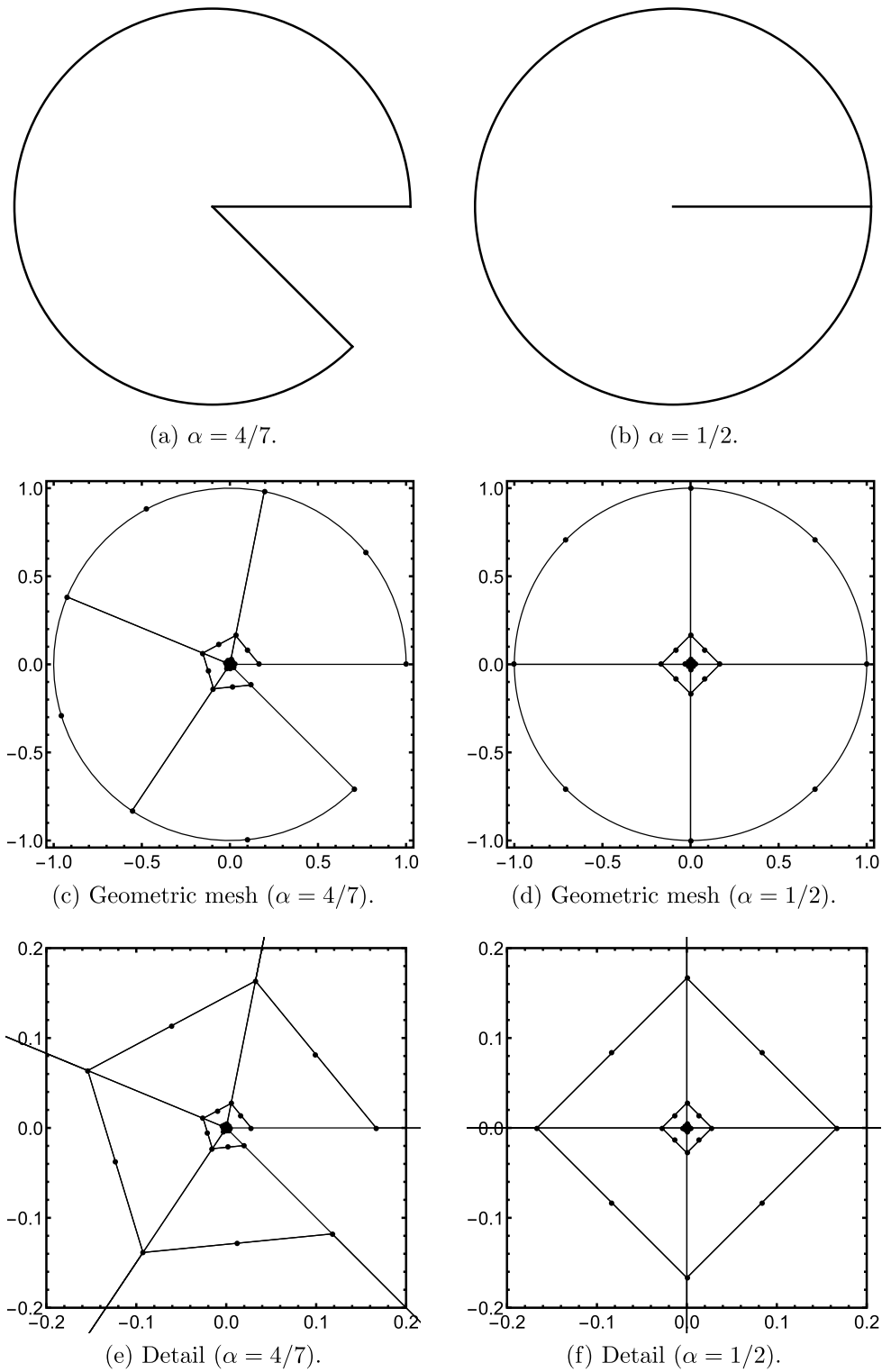


Fig. 7. Pacman domains with geometric meshes (including details around the singularity).

Exact values are not known. The reference values have been computed using the standard  $hp$ -FEM. The convergence within the sequence of spirals can be tested with the Weyl's Law [29]:

$$\lambda_k = \frac{4\pi}{|S_j|}(1 + o(1))k, \tag{12}$$

where  $|S_j|$  denotes the area of the  $j^{\text{th}}$  spiral in the sequence. From some index  $j$  on one expects the product  $|S_j|\lambda_1$ , say, remain constant. For the two sequences considered here, see Fig. 13.

Let us focus on eigenpairs  $(\lambda_1, u_1)$  and  $(\lambda_6, u_6)$  on both cases in the case of the complete spiral. Unlike in the case of the Pacman above, this choice is only to ensure continuity over the two sets of experiments. In Figs. 14 and 15 the eigenmodes are illustrated. In Figs. 16

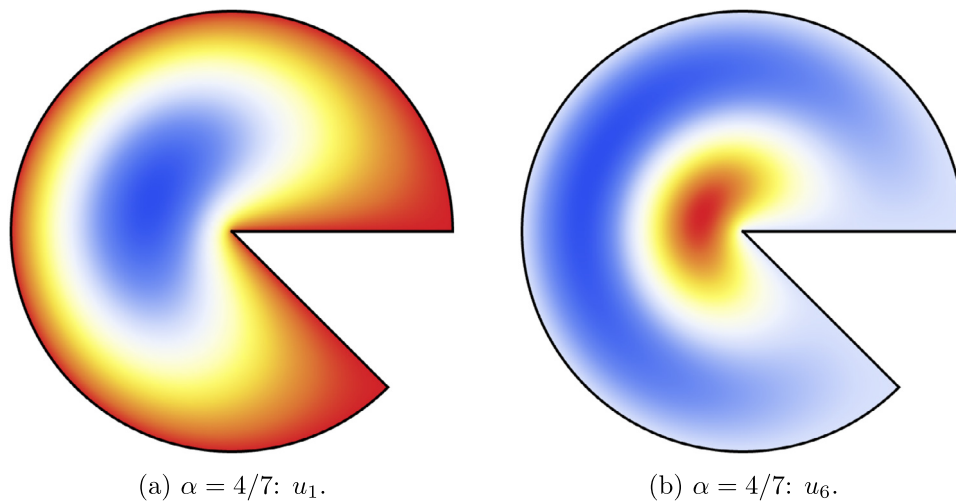


Fig. 8. Pacman modes. Temperature colour scaling.

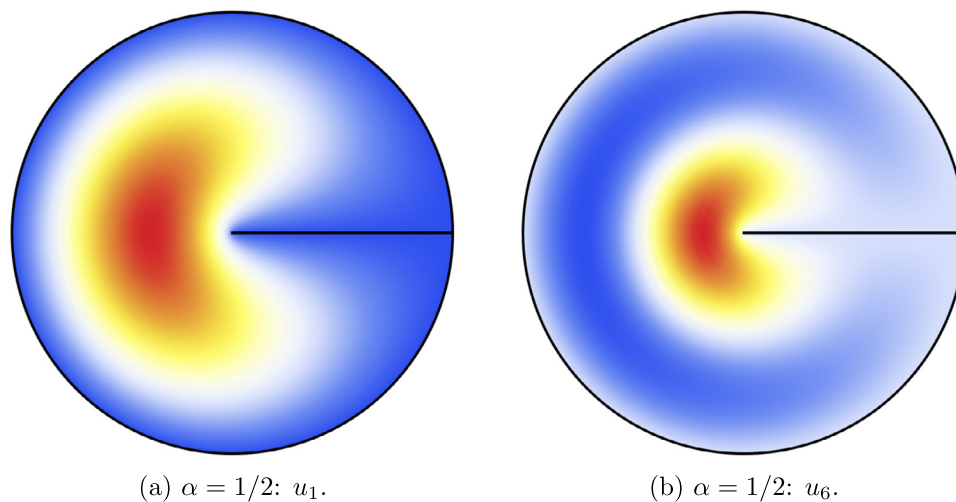


Fig. 9. Slit disk modes. Temperature colour scaling.

and 17 the estimated error is compared with the error against the computed reference values. In both cases the estimated error is optimistic. The convergence rate is not exponential, but reduces to algebraic as in the standard  $p$ -FEM. This is exactly as the theory predicts since there is no  $h$ -type refinement to any reentrant corner. This is not the result of poor resolution of the shape functions as is illustrated in the following.

#### 4.3. Effect of shape resolution

In this last case three convergence studies are repeated with a significantly higher resolution of the computed shape functions. For details, see Fig. 18. As mentioned above, in the case of constant coefficient problems, the error due to inaccurate evaluation of the shape functions is similar to normal quadrature error of the  $hp$ -FEM, say.

The results are summarised in Fig. 19. In the Pacman-problem where the observed convergence is exponential, it is not surprising that the improvement decreases as the polynomial degree increases. In the Padovan cases with the complete spiral, on the contrary, in the “pure- $p$ ”-setting the improvement grows with the polynomial degree.

In all cases the overall convergence characteristics are not altered and the graphs have not been repeated here. In the Pacman case the graphs are practically identical, however, in the Padovan cases with

Table 2

Pacman: Cost of refinement. Total time for integrating and assembling the stiffness and mass matrices. CPUtime in seconds as defined by Mathematica 13.3 `TimeUsed[]` on Macbook Pro (2022). If no shapes are precomputed, that is, reference data for different types is computed dynamically, the time for the stiffness matrix increases to 540 seconds in the minimal configuration.

	Stiffness	Mass	Total	Ratio
Minimal	240	218	458	1
Refined	3720	3567	7287	16

slower convergence one can observe slight changes at higher polynomial orders, and, indeed, fractionally better convergence rates. Notice that the improvements are increasing and thus affecting the rate, but only marginally.

#### 4.4. Computational complexity

If the shape function is computable, there must be a cost associated with them. Naturally, the higher levels of accuracy require more refined implementation meshes as has already been seen above. In

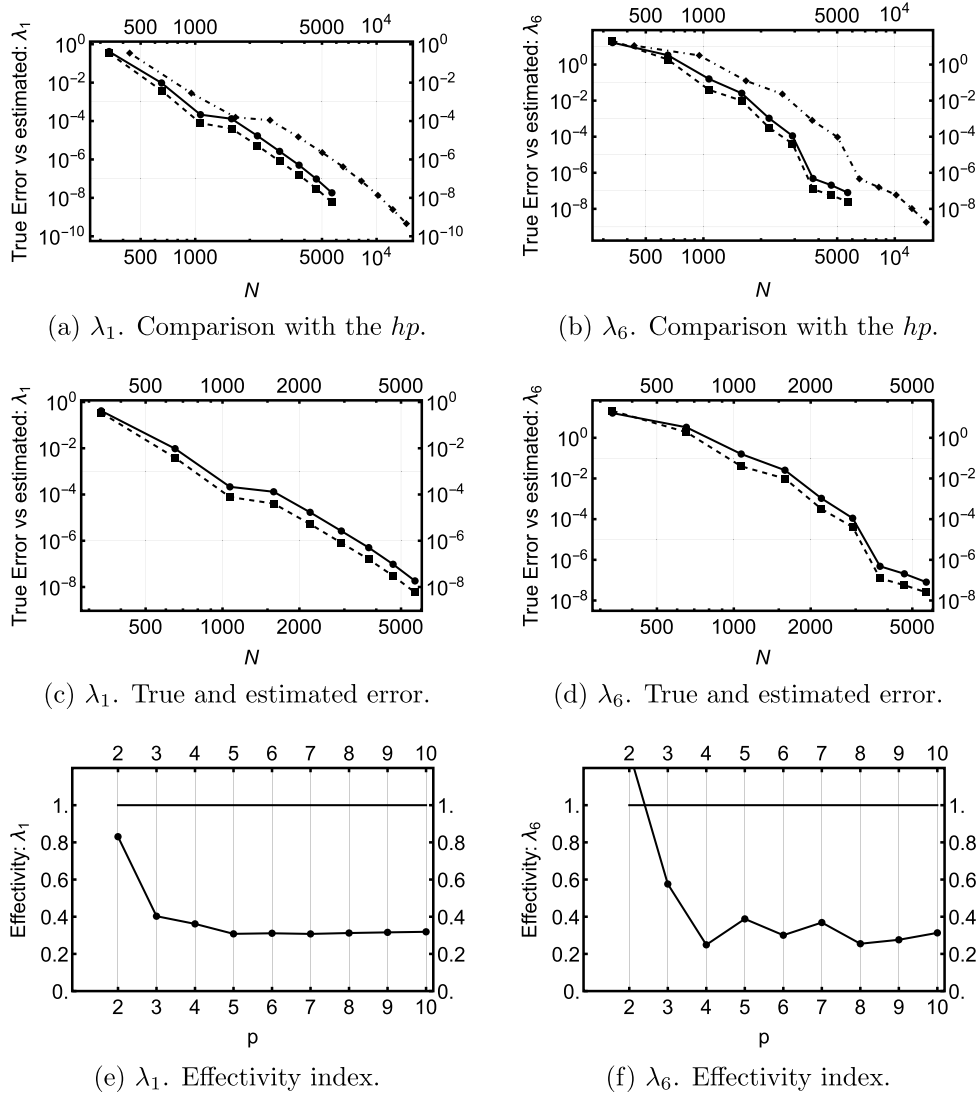


Fig. 10. Pacman convergence and effectivity indices. True errors over a  $p$ -sequence. Left column:  $\lambda_1$ ; Right column:  $\lambda_6$ . Convergence graphs: Dash-dotted line:  $hp$ , Solid line: harmonic extension, Dashed: estimated error.

Table 2 a breakdown of observed computation times (in synthetic time units on a multicore machine) over the whole integration and assembly sequence is given. In short: The extra decimals are expensive. The higher execution times simply reflect the composite quadrature rules on the implementation meshes (Fig. 18). This underlines the need for proper quadrature rules for these classes of functions. The moment fitting techniques used within the finite cell methods are one promising candidate [30]. (See also related ideas in [31], [32].)

### 5. Conclusions

The purpose of the new PDE discretisation methods is to provide for more flexibility in handling of the geometry or related tasks such as grading of the meshes to singularities or boundary layers. The harmonic extension elements, implemented via adaptive reference elements, is a non-intrusive extension of the  $p$ -version of FEM, and hence it inherits many of the properties such as exponential convergence if the mesh is properly graded. This flexibility comes with a cost, of course. The shape functions are computable harmonic functions, their inner products must be computed efficiently and therefore there has to be a shared implementation discretisation on which the existing finite element tech-

niques can be applied. Moreover, to our knowledge there are no results on optimal quadrature designs. The naive composite quadrature rules on implementation quadratures are very expensive and unavoidable if curved elements are used.

One of the advantages of non-intrusive approaches is that error estimation methods are readily available. In this paper, the auxiliary subspace error estimation is shown to perform on harmonic extension elements as expected, with convergence characteristics on eigenvalue problems aligned with those reported in connection of state-of-the-art  $hp$ -FEM methods.

The proposed method is constrained in the sense that the implementation is built on reference elements. It follows that the class of geometries one can handle is limited by the kind of mappings one can use. Of course, in principle one can always refine the meshes, but one of the fundamental properties of the underlying  $p$ -FEM is that large elements can be used.

The current implementation is for 2D only. By its design, the approach can be extended to 3D in a straightforward manner. However, the combinatorial explosion of the possible interface configurations on edges and faces means that initially only simple subdivisions should be admissible. In 2D the design of mappings and quadrature rules remains a challenge.

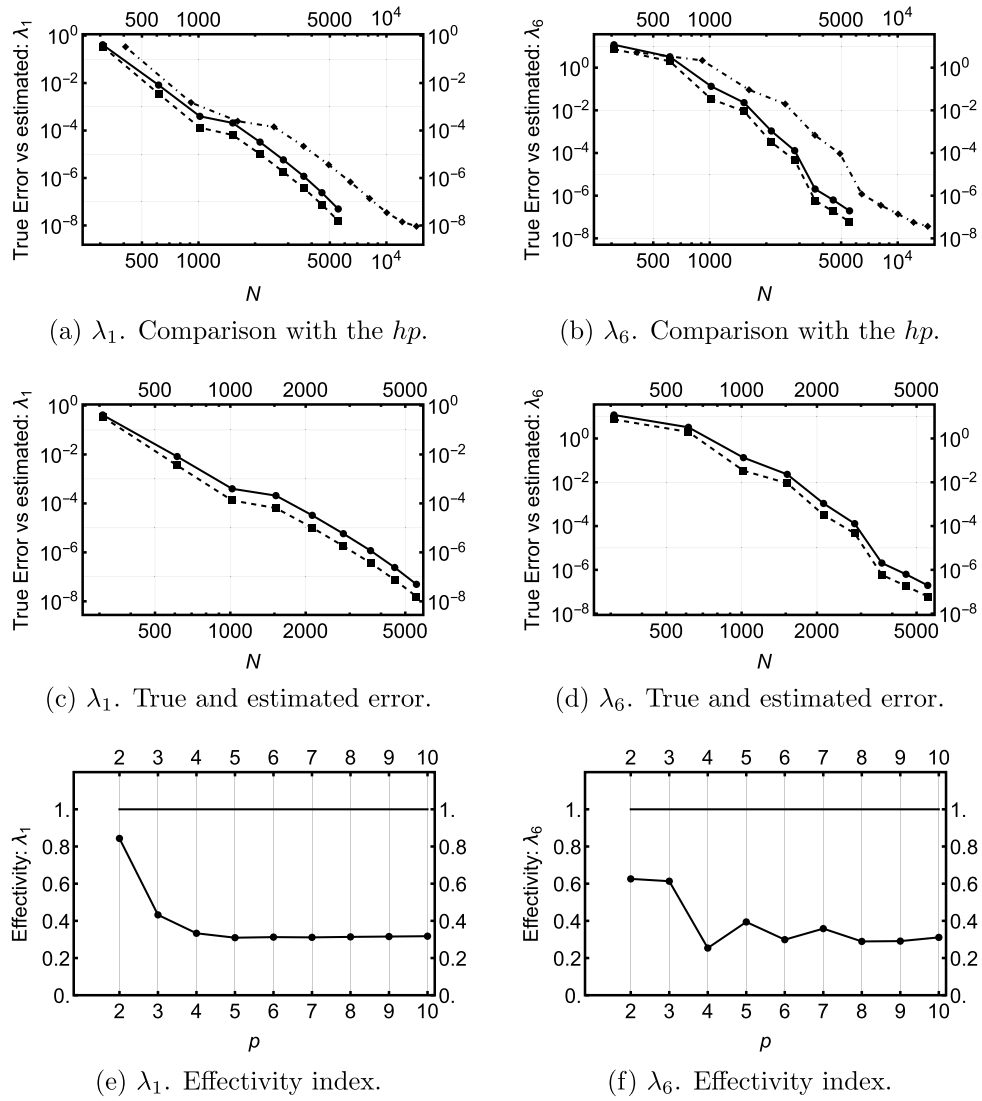


Fig. 11. Slit disk convergence and effectivity indices. True errors over a  $p$ -sequence. Left column:  $\lambda_1$ ; Right column:  $\lambda_6$ . Convergence graphs: Dash-dotted line:  $hp$ , Solid line: harmonic extension, Dashed: estimated error.

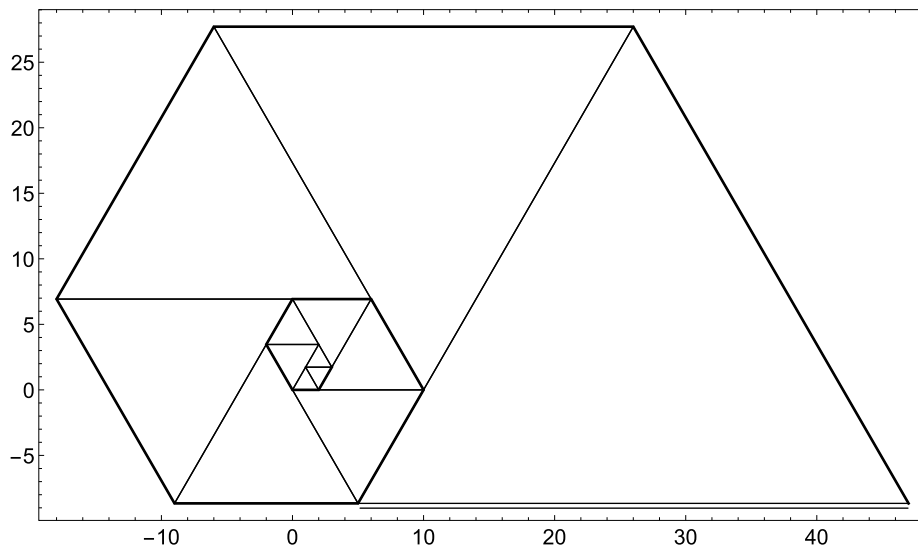


Fig. 12. Padovan sequence  $\{1, 1, 1, 2, 2, 3, 4, 5, 7, 9, 12, 16, 21\}$  illustrated. The unit length = 2. The Dirichlet boundary shared by both cases is shown with thick line. The boundary segment which is either Dirichlet or Neumann is indicated with a double line.

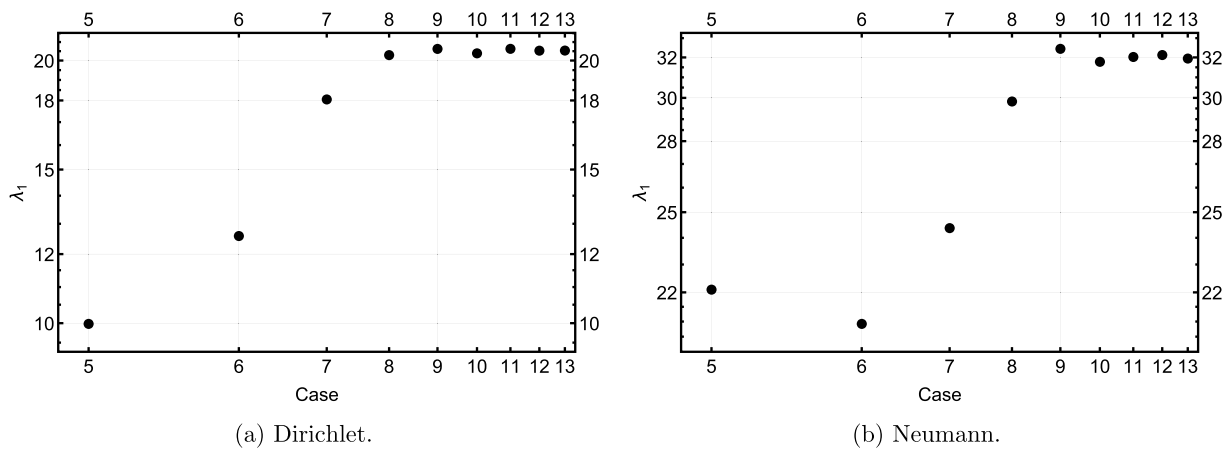


Fig. 13. Weyl's Law tested on the lowest mode over Padovan Spirals. The asymptotic sequence starts on the 9th and 8th for the Dirichlet and Neumann sequences, respectively.

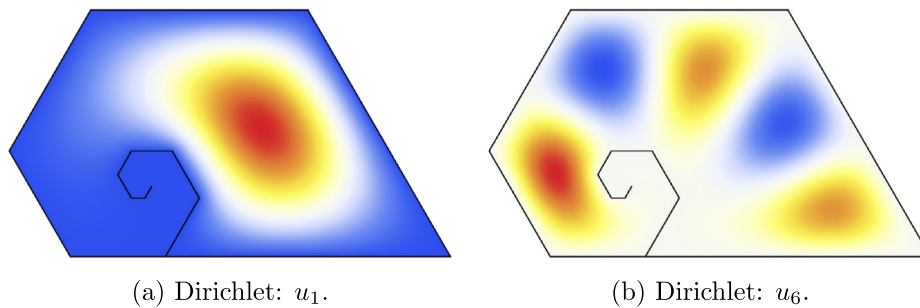


Fig. 14. Dirichlet Padovan Spiral:  $u_1$  and  $u_6$ .

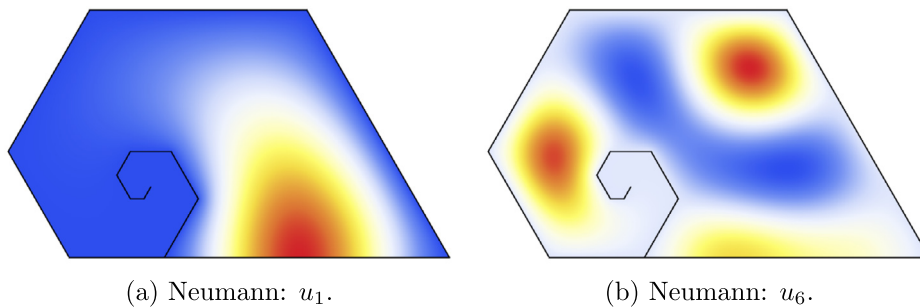


Fig. 15. Neumann Padovan Spiral:  $u_1$  and  $u_6$ .

Data availability

No data was used for the research described in the article.

References

[1] L. Beirão da Veiga, F. Brezzi, A. Cangiani, G. Manzini, L.D. Marini, A. Russo, Basic principles of virtual element methods, *Math. Models Methods Appl. Sci.* 23 (2013) 199–214.

[2] D.A. Di Pietro, J. Droniou, *The Hybrid High-Order Method for Polytopal Meshes*, Springer, 2020.

[3] E. Burman, S. Claus, P. Hansbo, M.G. Larson, A. Massing, CutFEM: discretizing geometry and partial differential equations, *Int. J. Numer. Methods Eng.* 104 (2015) 472–501.

[4] E. Burman, P. Hansbo, M.G. Larson, CutFEM based on extended finite element spaces, *Numer. Math.* 152 (2022) 331–369.

[5] M. Dauge, A. Düster, E. Rank, Theoretical and numerical investigation of the finite cell method, *J. Sci. Comput.* 65 (2015).

[6] B. Marussig, J. Zechner, G. Beer, T.P. Fries, Stable isogeometric analysis of trimmed geometries, *Comput. Methods Appl. Mech. Eng.* 316 (2017).

[7] T.Y. Hou, X.-H. Wu, Z. Cai, Convergence of a multiscale finite element method for elliptic problems with rapidly oscillating coefficients, *Math. Comput.* 68 (1999) 913–943.

[8] M. Oleksy, W. Cecot, W. Rachowicz, M. Nessel, An improved multiscale fem for the free vibrations of heterogeneous solids, *Comput. Math. Appl.* 110 (2022) 110–122.

[9] B. Szabo, I. Babuska, *Finite Element Analysis*, Wiley, 1991.

[10] C. Schwab, *p- and hp-Finite Element Methods*, Oxford University Press, 1998.

[11] H. Hakula, Adaptive reference elements via harmonic extensions and associated inner modes, *Comput. Math. Appl.* 80 (2020) 2272–2288.

[12] H. Hakula, Resolving boundary layers with harmonic extension finite elements, *Math. Comput. Appl.* 27 (2022).

[13] C. Hofreither, U. Langer, S. Weißer, Convection-adapted BEM-based FEM, *ZAMM, Z. Angew. Math. Mech.* 96 (2016) 1467–1481.

[14] S. Weißer, Arbitrary order Trefftz-like basis functions on polygonal meshes and realization in BEM-based FEM, *Comput. Math. Appl.* 67 (2014) 1390–1406.

[15] J.S. Owall, S.E. Reynolds, A high-order method for evaluating derivatives of harmonic functions in planar domains, *SIAM J. Sci. Comput.* 40 (2018) A1915–A1935.

[16] A. Anand, J.S. Owall, S.E. Reynolds, S. Weißer, Trefftz finite elements on curvilinear polygons, *SIAM J. Sci. Comput.* 42 (2020) A1289–A1316.

[17] L. Demkowicz, J. Gopalakrishnan, A primal DPG method without a first-order reformulation, *Comput. Math. Appl.* 66 (2013) 1058–1064.

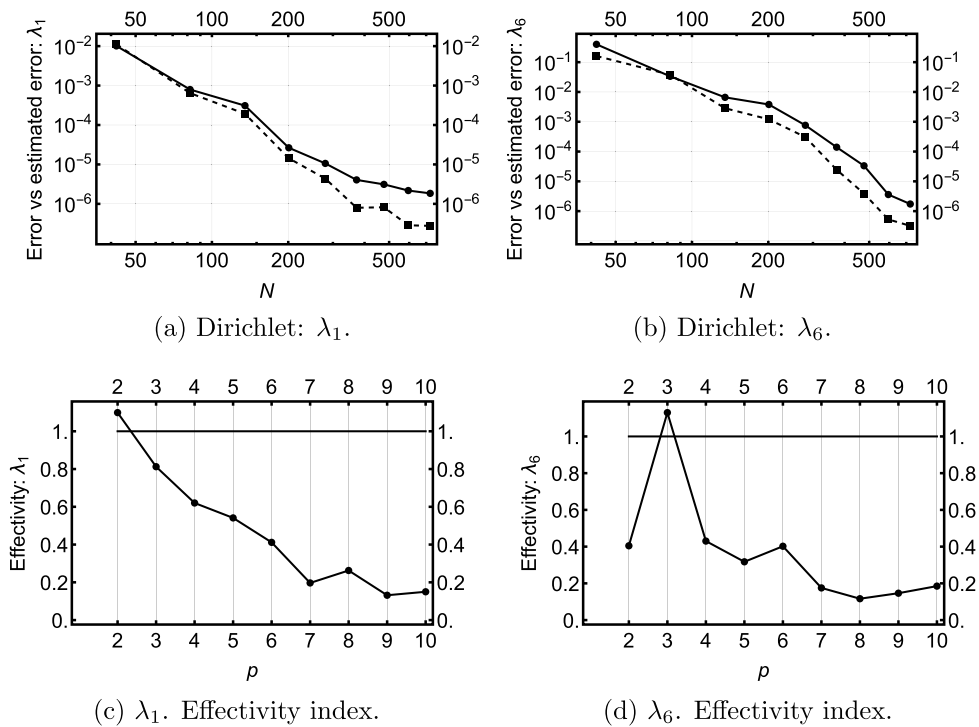


Fig. 16. Dirichlet Padovan Spiral:  $\lambda_1$  and  $\lambda_6$ . The error based on the computed reference (solid line) vs the estimated error (dashed line).

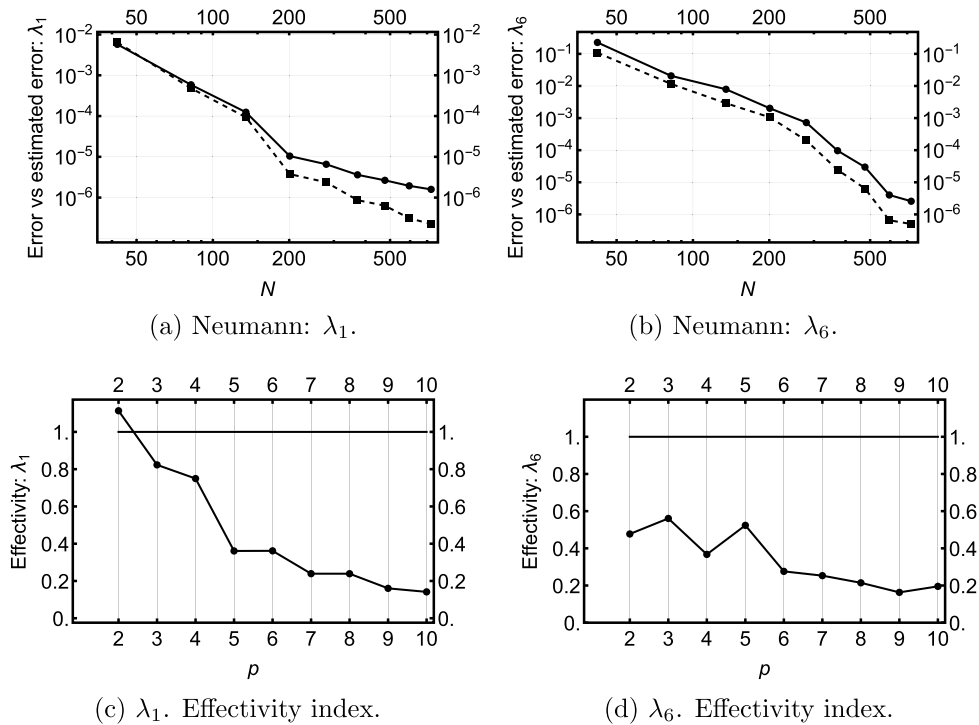


Fig. 17. Neumann Padovan Spiral:  $\lambda_1$  and  $\lambda_6$ . The error based on the computed reference (solid line) vs the estimated error (dashed line).

[18] W.J. Gordon, C.A. Hall, Transfinite element methods: blending function interpolation over arbitrary curved element domains, *Numer. Math.* 21 (1973) 109–129.

[19] H. Hakula, T. Quach, A. Rasila, Conjugate function method for numerical conformal mappings, *J. Comput. Appl. Math.* 237 (2013) 340–353.

[20] Wolfram Research, Inc., *Mathematica*, Version 13.3.1, 2023, Champaign, IL.

[21] H. Hakula, T. Tuominen, Mathematica implementation of the high order finite element method applied to eigenproblems, *Computing* 95 (2013) 277–301.

[22] H. Hakula, M. Neilan, J.S. Owall, A posteriori estimates using auxiliary subspace techniques, *J. Sci. Comput.* 72 (2017) 97–127.

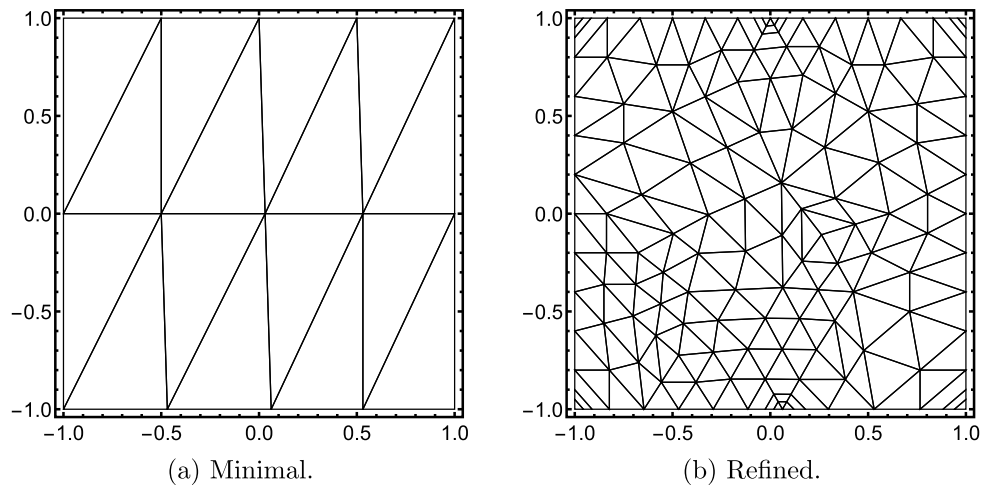
[23] S. Giani, L. Grubišić, H. Hakula, J. Owall, A posteriori error estimates for elliptic eigenvalue problems using auxiliary subspace techniques, *J. Sci. Comput.* 88 (2021).

[24] S. Henneking, L. Demkowicz, *hp3D User Manual*, <https://doi.org/10.48550/arXiv.2207.12211>, 2023.

[25] P. Solin, K. Segeth, I. Dolezel, *Higher Order Finite Element Methods*, har/cdr edition, Chapman and Hall/CRC, 2003.

[26] J.R. Kuttler, V.G. Sigillito, Eigenvalues of the Laplacian in two dimensions, *SIAM Rev.* 26 (1984) 163–193.

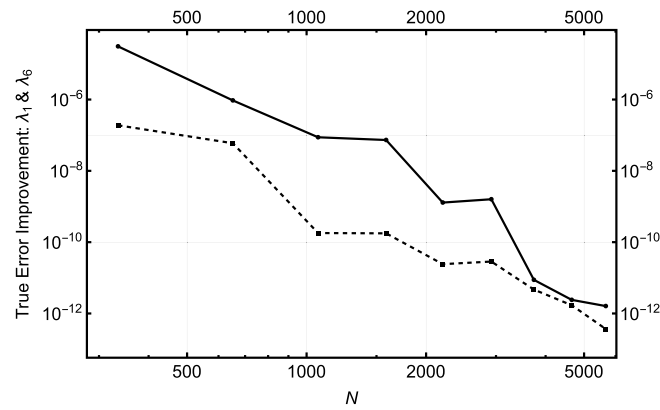
[27] I. Stewart, *Math Hysteria: Fun and Games with Mathematics*, Oxford University Press, 2004.



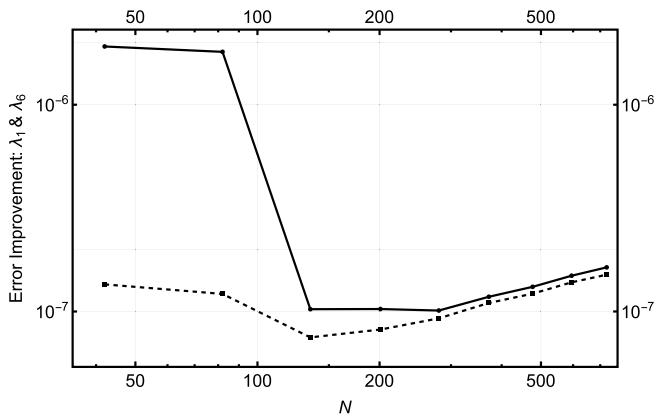
	N	E	T	Q	#DOF
Minimal	15	30	16	-	1225
Refined	156	379	204	20	17965

(c) Discretisation data.

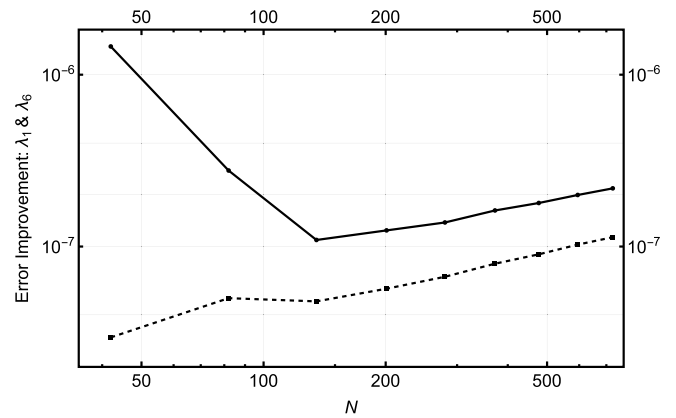
Fig. 18. Two implementation meshes used in Pacman problem for a quadrilateral adaptive reference element.



(a) Pacman:  $\alpha = 4/7$ .



(b) Padovan: Dirichlet.



(c) Padovan: Neumann.

Fig. 19. Improvement in the error due to higher resolution of the shape functions. For the Pacman, the true error is measured, whereas for the two Padovan cases, the error based on the computed reference is considered. Solid line:  $\lambda_6$ , Dashed line:  $\lambda_1$ .

- [28] R. Padovan, Dom Hans van der Laan: Modern Primitive, Architectura & Natura Press, 1994.
- [29] H. Weyl, Über die Asymptotische Verteilung der Eigenwerte, Nachrichten der Königlichen Gesellschaft der Wissenschaften zu Göttingen, 1911, pp. 110–117.
- [30] W. Garhuom, S. Hubrich, L. Radtke, A. Düster, Adaptive Quadrature and Remeshing Strategies for the Finite Cell Method at Large Deformations, Springer International Publishing, Cham, 2022, pp. 327–353.
- [31] Y. Sudhakar, W.A. Wall, Quadrature schemes for arbitrary convex/concave volumes and integration of weak form in enriched partition of unity methods, Comput. Methods Appl. Mech. Eng. 258 (2013) 39–54.
- [32] B. Müller, F. Kummer, M. Oberlack, Highly accurate surface and volume integration on implicit domains by means of moment-fitting, Int. J. Numer. Methods Eng. 96 (2013) 512–528.